Optimization of a Table-top X-ray Fluorescence Computed Tomography (XFCT) system

Chelsea Dunning & Magdalena Bazalova-Carter
University of Victoria

X-ray Cancer Imaging and Therapy Experimental LAB

Emerging and Preclinical Modalities:
Sunday, July 29 at 4:00 PM - 4:20 PM
Davidson Ballroom B

Significance

We are designing a table-top XFCT system that will use combined K-shell and L-shell fluorescent x-rays (FX) to image heavy-atomic number nanoparticles in small animal-sized objects using four cadmium telluride (CdTe) and four silicon drift diode (SDD) spectrometers. Our XFCT system will allow the combined benefit of **high-sensitivity L-shell XFCT** and **penetrating K-shell XFCT**. The use of multiple spectrometers in a pencil beam scan will enable **faster scanning while preserving XFCT image quality** compared to single-spectrometer scans.

Careful thought must be put into the arrangement of the spectrometers. Detecting backscattered FXs relative to the incident pencil beam improves contrast-to-noise ratio (CNR) of K-shell XFCT images by an order of magnitude relative to isotropic FXs[1] in a single-spectrometer scan. L-shell XFCT can also achieve higher CNR when imaging low nanoparticle concentrations compared to K-shell XFCT[2]. This work modelled a pencil beam scan of a small animal water phantom loaded with gold nanoparticles (AuNP) and realistic data acquisition using CdTe and SDD spectrometers. We explored the effect of three different spectrometer arrangements, K-shell versus L-shell XFCT imaging, two different CdTe detector crystal sizes, and two different detector-surface distances (DSD) on the resulting image quality. We will also determine at what AuNP vial depth would the image quality of L-shell XFCT overtake K-shell XFCT.

Methods

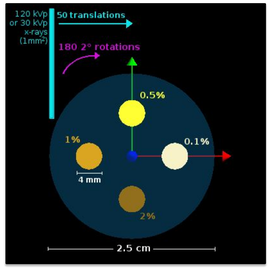

Cross-sectional diagram of the 2.5cm diameter cylindrical water phantom modelled in TOPAS, a Monte Carlo software package. All dimensions are shown with the AuNP vial locations at various concentrations by weight of gold. The 1x1 mm² pencil beam enters the phantom from the top, which scans the phantom in 50 0.5mm-steps and 180 2°-rotations and delivers a dose of 30 mGy.

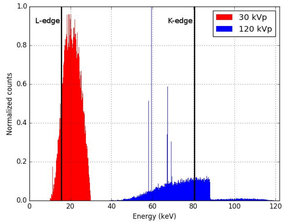

Primary beam energy spectra of the 1mm Al-filtered 30 kVp and 0.5mm Pb-filtered 120 kVp pencil beam x-ray source used for prompt irradiation of the phantom. Only prompt x-rays that are above the L-edge and K-edge in each source are useful for generating L-shell and K-shell FXs in the AuNPs, respectively. Each source was generated by a separate simulation of an x-ray tube and collimated to a 1x1 mm² beam area using a tungsten collimator.

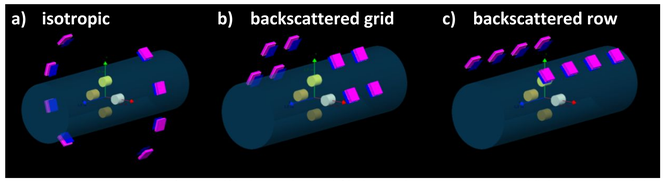

Spectrometer arrangements, namely **a) isotropic, b) backscattered grid, and c) backscattered row arrangements**, are modelled in TOPAS along with the water phantom and loaded AuNP vials. The term 'backscattered' is relative to the primary x-ray beam, which enters the phantom from the top. Shown here are the Amptek X-123 CdTe spectrometers, which are suitable for K-shell XFCT. The Amptek X-123 SDD spectrometers, suitable for lower-energy L-shell XFCT, are not pictured but arranged similarly. The spectrometers in both backscattered detector arrangements here are placed 1 cm away from the phantom surface. Due to geometric constraints, the spectrometers in the isotropic detector arrangement are placed 1.3 cm away from the phantom surface.

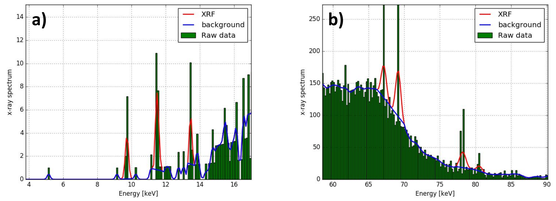

Sample detected x-ray spectrum showing **a) L-shell** and **b) K-shell** FX signal extraction for a single projection. The simulated spectrum is corrected for detector response using the stripping method[3]. Next, the corrected spectrum is convoluted with a gaussian of FWHM 200 eV and 900 eV to model the energy resolution of the SDD and CdTe spectrometers, respectively, to mimic the x-ray spectrum the spectrometer would realistically detect. The background is then subtracted from the FX signal, as shown. The number of counts in the signal is stored for this particular rotation and translation in a projection map known as a sinogram.

Conclusion

The backscattered grid detector arrangement is the optimal arrangement with the lowest minimum concentration of AuNP detectable for both K-shell and L-shell XFCT imaging. **These simulated results will guide our design for our new bench-top XFCT imaging system**, which will enable faster imaging of heavy-atomic number nanoparticles loaded in small animal-sized objects.

[1] Ahmad M, Bazalova M, Xiang L, Xing L. Order of magnitude sensitivity increase in x-ray fluorescence computed tomography (XFCT) imaging with an optimized spectro-spatial detector configuration: theory and simulation. *IEEE Trans Med Imaging*. 2014;**33**:1119–1128.
[2] Bazalova M, Ahmad M, Pratx G, Xing L. L-shell x-ray fluorescence computed tomography (XFCT) imaging of Cisplatin. *Phys Med Biol.* 2014;**59**:219–232.
[3] Seltzer S M 1981 Calculated response of intrinsic germanium detectors to narrow beams of photons with energies up to ~300 keV *Nucl. Instrum. Methods* **188** 133–51
[4] Rose A. Vision: Human and Electronic. New York, NY: Plenum; 1973.

Results

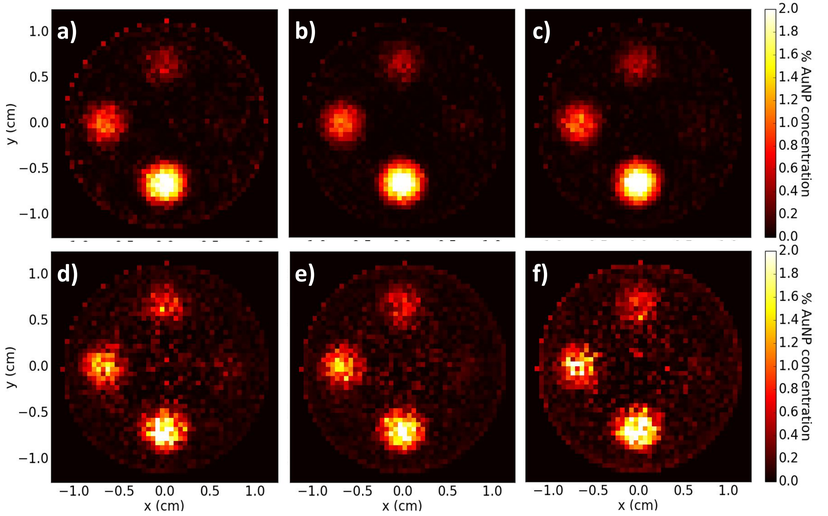

Reconstructed images for the **(a,d) isotropic**, **(b,e) backscattered grid**, and **(c,f) backscattered row detecto**r arrangements using **(a-c) K-shell** and **(d-f) L-shell** XFCT. The L-shell XFCT images were corrected for x-ray attenuation. Each image was reconstructed using an iterative reconstruction algorithm known as the Maximum-Likelihood Expectation Maximization (MLEM) algorithm, and normalized to the mean signal of the 2% AuNP vial.

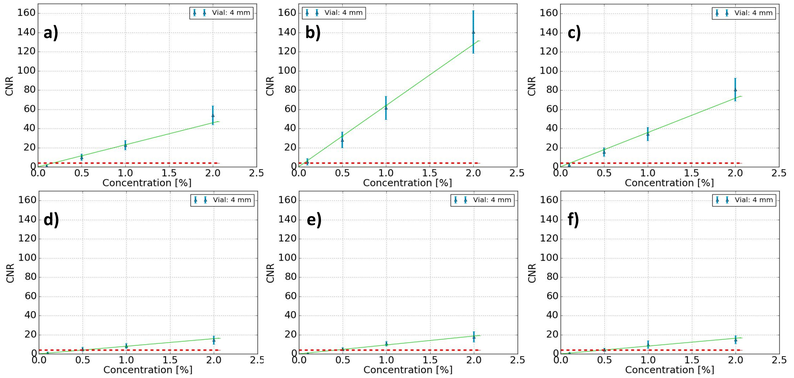

AuNP concentration vs. CNR plots of the **(a-c) K-shell** and **(d-f) L-shell** XFCT images above for the **a,d) isotropic, b,e) backscattered grid**, and **c,f) backscattered row** detector arrangements. The Rose criterion[4] (CNR = 4) is shown as a red dashed line. The CNR for each vial was determined by taking the mean signal in each vial, subtracting the signal in the background, and then dividing by the standard deviation of the background. The background region of interest was defined as a central circle of diameter 0.5 cm in the middle of the water phantom. Out of the K-shell XFCT images, there is quite a difference in the CNR between all three detector arrangements, whereas the difference is less pronounced out of the L-shell XFCT images. The backscattered grid detector arrangement has the highest CNR in the K-shell and L-shell XFCT images.

	Isotropic		Backscattered grid		Backscattered row	
	Minimum % AuNP	CNR of 2% vial	Minimum % AuNP	CNR of 2% vial	Minimum % AuNP	CNR of 2% vial
K-shell XFCT	0.17%	53	**0.06%**	**140**	0.11%	80
L-shell XFCT	0.50%	13	**0.43%**	**18**	0.49%	15

Summary of results showing the minimum AuNP concentrations detectable and CNR of the highest AuNP concentration vial for each of the K-shell and L-shell XFCT images at each of their detector arrangements. The minimum detectable AuNP concentration was determined by fitting a linear function to each of the AuNP concentration vs. CNR plots above, and determining the concentration value at the Rose criterion of CNR = 4.